

## Mechanism, Reactivity, and Selectivity in Palladium-Catalyzed Redox-Relay Heck Arylations of Alkenyl Alcohols

Liping Xu,<sup>†</sup> Margaret J. Hilton,<sup>‡</sup> Xinhao Zhang,<sup>†</sup> Per-Ola Norrby,<sup>\*,§,||</sup> Yun-Dong Wu,<sup>\*,†</sup> Matthew S. Sigman,<sup>\*,‡</sup> and Olaf Wiest<sup>\*,†,⊥</sup><sup>†</sup>Lab of Computational Chemistry and Drug Design, Laboratory of Chemical Genomics, Peking University Shenzhen Graduate School, Shenzhen 518055, China<sup>‡</sup>Department of Chemistry, University of Utah, 315 South 1400 East, Salt Lake City, Utah 84112, United States<sup>§</sup>Department of Chemistry and Molecular Biology, University of Gothenburg, Kemigården 4, SE 412 96 Göteborg, Sweden<sup>||</sup>Pharmaceutical Development, Global Medicines Development, AstraZeneca, Pepparedsleden 1, SE-431 83 Mölndal, Sweden<sup>⊥</sup>Department of Chemistry and Biochemistry, University of Notre Dame, Notre Dame, Indiana 46556-5670, United States

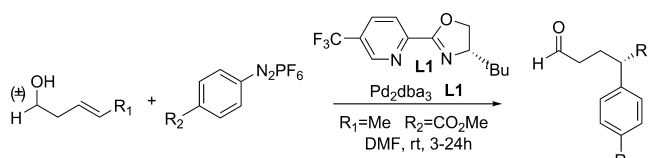
## Supporting Information

**ABSTRACT:** The enantioselective Pd-catalyzed redox-relay Heck arylation of acyclic alkenyl alcohols allows access to various useful chiral building blocks from simple olefinic substrates. Mechanistically, after the initial migratory insertion, a succession of  $\beta$ -hydride elimination and migratory insertion steps yields a saturated carbonyl product instead of the more general Heck product, an unsaturated alcohol. Here, we investigate the reaction mechanism, including the relay function, yielding the final carbonyl group transformation. M06 calculations predict a  $\Delta\Delta G^\ddagger$  of 1 kcal/mol for the site selectivity and 2.5 kcal/mol for the enantioselectivity, in quantitative agreement with experimental results. The site selectivity is controlled by a remote electronic effect, where the developing polarization of the alkene in the migratory insertion transition state is stabilized by the C–O dipole of the alcohol moiety. The enantioselectivity is controlled by steric repulsion between the oxazoline substituent and the alcohol-bearing alkene substituent. The relay efficiency is due to an unusually smooth potential energy surface without high barriers, where the hydroxyalkyl-palladium species acts as a thermodynamic sink, driving the reaction toward the carbonyl product. Computational predictions of the relative reactivity and selectivity of the double bond isomers are validated experimentally.

## INTRODUCTION

The Heck reaction is an excellent method to introduce an aromatic group to one end of a double bond using palladium-catalysis.<sup>1,2</sup> The asymmetric variant of the Heck reaction has received great attention as it generates chiral centers when forming new carbon–carbon bonds, of vast importance in natural product and pharmaceutical syntheses.<sup>3–5</sup> One of the most significant limitations is the requirement of a biased alkene, such as a styrene or an  $\alpha,\beta$ -unsaturated carbonyl, in order to achieve high regiocontrol of the initial migratory insertion and the resultant  $\beta$ -hydride elimination of the formed Pd-alkyl intermediate. Another strategy for achieving selectivity in Heck reactions is to use alkenes with adjacent coordinating or directing groups,<sup>6–13</sup> which has been applied in decarboxylative<sup>14</sup> and oxidative<sup>15–20</sup> Heck reactions to achieve high site selectivity. Sigman and others reported a highly regioselective Heck reaction of electronically nonbiased alkenes without chelating groups.<sup>18,21–23</sup> Very recently, Sigman and co-workers reported a highly enantioselective redox-relay Heck arylation of acyclic alkenol alcohols (Scheme 1). They reported the use of aryl diazonium salts<sup>24</sup> and, more recently, an oxidative variant employing aryl boronic acid derivatives<sup>25</sup> as the coupling partners. Both deliver remotely functionalized carbonyl products in high enantioselectivity and with fair to excellent site selectivity, depending on the reactant combinations. The newly formed carbonyl group is remote from the site of carbon–carbon bond formation, which suggests a chain-

## Scheme 1. Heck Arylation of Acyclic Alkenol Alcohols and Aryl Diazonium Salts



walking process of the Pd-catalyst species to ultimately transform the unsaturation of the alkene to the alcohol.<sup>26–31</sup> This type of reaction is very attractive for two reasons: first, it occurs with generally high site selectivity and enantioselectivity with unbiased achiral substrates; and second is the simultaneous functionalization of multiple carbons through a presumably iterative  $\beta$ -hydride elimination/migratory insertion process.

The Heck reaction has been well-studied theoretically, most frequently using the B3LYP functional.<sup>22,23,32–41</sup> Many studies have focused on the main selectivity-determining step, the migratory insertion.<sup>19,20,42–44</sup> In addition, the  $\beta$ -hydride elimination step that is an important feature of the current reaction has also been investigated.<sup>30,31</sup> For asymmetric Heck reactions, previous studies have focused on cyclic sub-

Received: October 27, 2013

Published: January 11, 2014

strates.<sup>32,45</sup> However, to our knowledge, the more complex situation, where asymmetry is induced in an open-chain alkene, has not been studied theoretically. To this end, we have carried out a mechanistic study on the title reaction using density functional theory methods. These calculations provide a complete picture of the mechanism and a rationalization of the observed site-selectivity and enantioselectivity for this unique variant of the Heck reaction.

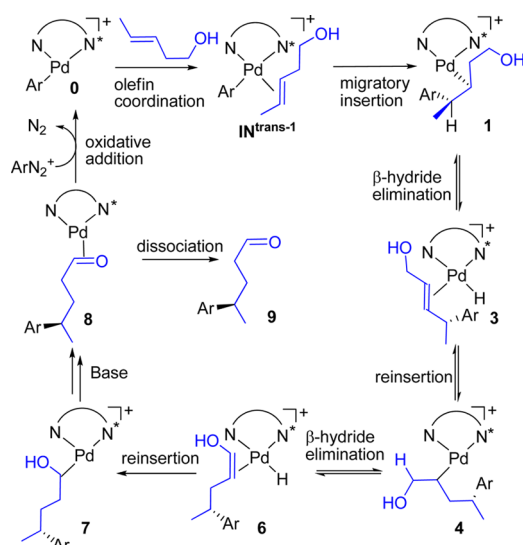
## ■ COMPUTATIONAL DETAILS

As a model system to elucidate the mechanism, we studied the reaction shown in Scheme 1. The computational methodology was benchmarked using a series of hybrid and dispersion corrected density functionals (Table S1 in the Supporting Information [SI]). It was found that the results for the six dispersion corrected functionals tested are very similar. Throughout the manuscript, the results from unconstrained geometry optimizations using the M06 functional<sup>46</sup> implemented in Gaussian09<sup>47</sup> are reported. This functional includes corrections for dispersion interactions and was found to be reliable for studies of Heck<sup>43</sup> and related reactions.<sup>45,48</sup> The LanL2DZ and 6-31+G(d) basis sets were used for Pd and all other atoms, respectively. Single point calculations using the SDD basis set for Pd and the 6-311++G(d, p) basis set for all other atoms and the SMD solvent model with the parameters for DMF were used to account for solvent effects. Frequency calculations at the same level of theory at the optimized geometries confirmed the stationary points as minima (zero imaginary frequencies) or transition state (one imaginary frequency) and provided the thermal corrections to the single point energies. Several conformations for each of the species have been investigated but only the results for the lowest energy conformer are presented. The final free energies from the single point calculations with solvent and thermal corrections are reported in kcal/mol. For clarity, the charge state of this cationic reaction is not shown in some Figures. Partial charges with hydrogens summed into the carbons they are attached to were calculated using the NBO Charge Analysis.

## ■ RESULTS AND DISCUSSION

**The Catalytic Cycle.** The proposed catalytic cycle of the asymmetric Heck redox-relay arylation is shown in Scheme 2. It begins with oxidative addition of an aryl diazonium salt to a Pd(0) species to form an aryl–Pd(II) complex *in situ*. This complex may have two possible structures, with the aryl group

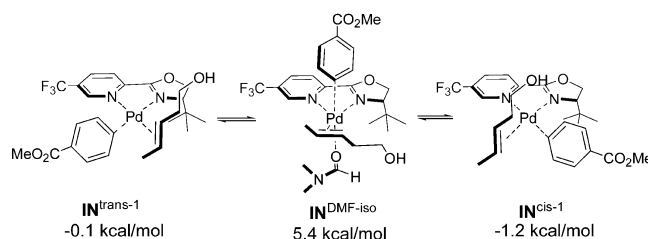
**Scheme 2. Catalytic Cycle of the Asymmetric Heck Redox-Relay Reaction**



positioned either *trans* or *cis* to the chiral oxazoline on the ligand. The perpendicular coordination of homoallylic alcohols to the Pd(II) species may occur from two different prochiral faces. On each face, the substituted methyl group can be positioned either below the “square plane”, proximal to the *tert*-butyl group, or above the “square plane”, distal from the *tert*-butyl group. As a result, a total number of eight conceivable isomeric Pd(II)– $\pi$ -alkene species needs to be considered. The next steps are alkene insertion into the Pd–aryl bond to deliver the Pd(II)–alkyl species and  $\beta$ -hydride elimination to form a hydrido–palladium alkene species. Subsequent repetition of the reinsertion and  $\beta$ -hydride elimination sequence gives a hydroxyalkyl–palladium species, which after deprotonation regenerates the Pd(0) species ligated to the carbonyl. This complex can either dissociate to give the final product and regenerate the catalyst or possibly react first with another equivalent of the aryl diazonium salt before liberating the product and closing the catalytic cycle.

**Isomerization of the Initial Intermediates.** The starting aryl–palladium(II) alkene intermediate (structure **IN<sup>trans-1</sup>** in Scheme 2) has two possible configurations, with the aryl group positioned either *trans* or *cis* to the chiral oxazoline on the ligand. Holder et al studied the *trans*–*cis* isomerization of the tricoordinated arylpalladium(II) and showed that the isomerization via a dissociative mechanism has a high activation free energy.<sup>48</sup> However, it is well-known that *cis*–*trans* isomerization can be strongly accelerated by basic ligands like chloride<sup>49,50</sup> or phosphines.<sup>51</sup> We therefore tested the hypothesis that the same type of process could be initiated by the coordination of the solvent, DMF. Our calculations show a feasible, low-energy path through an associative mechanism (**IN<sup>DMF-iso</sup>**, Scheme 3) by the coordination of an

**Scheme 3. Isomerization of Starting Intermediates with Associated Mechanism**



additional DMF molecule. Analogous to earlier studies (e.g., ref 52), we were unable to locate the TS for this isomerization, presumably due to the complex coordinate of the Berry pseudorotation. However, the relatively low free energy of the trigonal bipyramidal intermediate (5.4 kcal/mol), together with the results from the earlier studies discussed above, indicates a potential isomerization pathway. With a rapidly isomerizing starting complex, the migratory insertion should be under Curtin–Hammett control and, thus, be solely dictated by the relative energies of the competing insertion transition states. We note that under conditions where a similar aryl–Pd species is configurationally stable, Holder et al.<sup>48</sup> noted a significant decrease in enantioselectivity, indicating that under catalytic conditions, the intermediate *can* isomerize rapidly. As in our case, they also failed to locate the TS of the transformation, attesting to the complexity of the isomerization path.

**Free Energy Profiles and the Relay Strategy.** The computed Gibbs free energy surface for the Pd-catalyzed redox

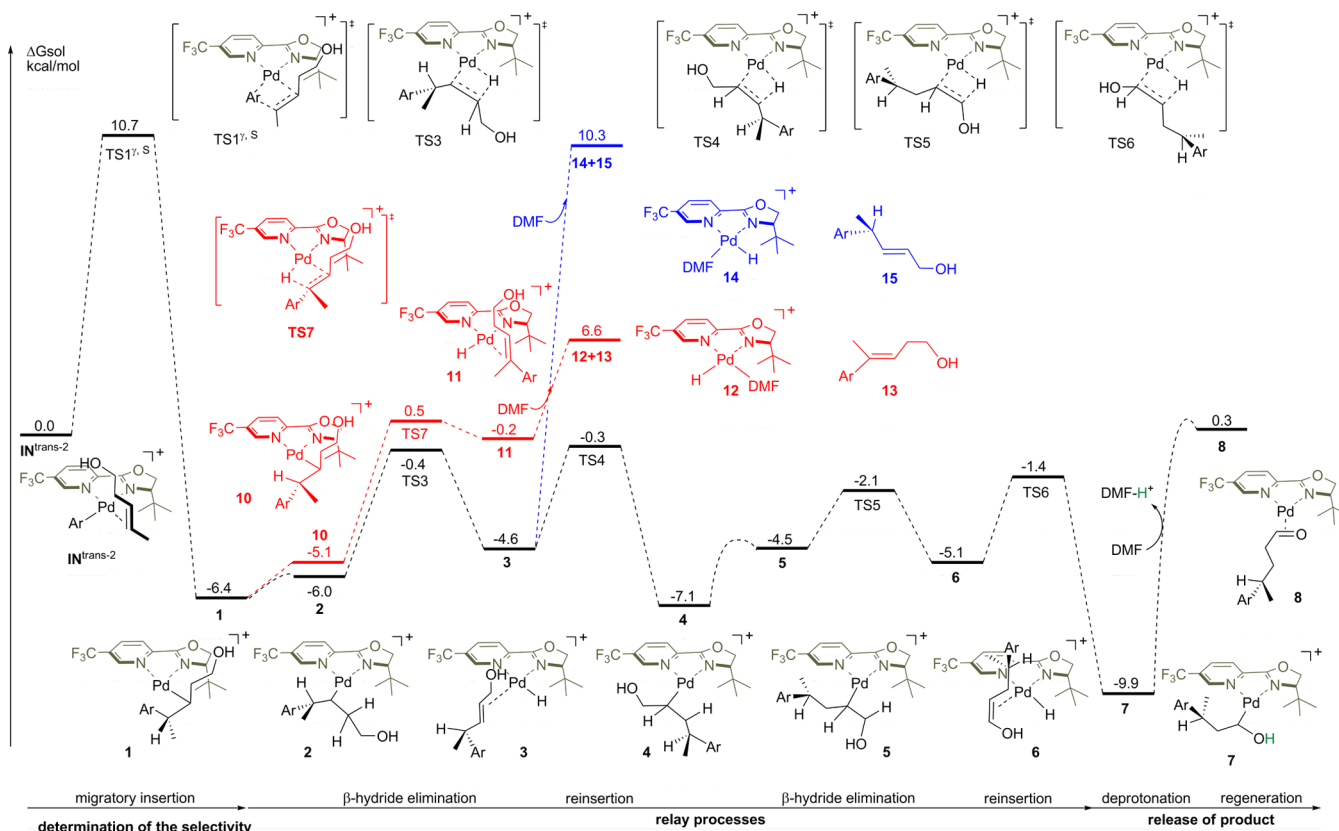


**Figure 1.** Potential energy surface of the reaction pathway, the alternative conventional Heck reaction pathway (via TS7, shown in red), and the direct alkene dissociation pathway (shown in blue).

relay Heck reaction of (*E*)-pent-3-en-1-ol with *p*-carboxymethoxyphenyl diazonium salt is shown in Figure 1 with the low energy pathway depicted in black. Previous electrospray and tandem mass spectrometry studies<sup>53,54</sup> of the Heck reaction have shown that the oxidative addition of aryl diazonium salts to palladium is very fast. Recent computational studies on the Pd-catalyzed conjugated addition of aryl boronic acids to  $\beta$ -substituted cyclic enones also showed this step as well as the coordination of the olefin to be facile.<sup>48</sup> Finally, the reaction can also be performed using aryl boronic acids as the source of the aryl group.<sup>25</sup> Therefore, we started our investigation from the Pd(II)-aryl alkene alcohol species  $\text{IN}^{\text{trans-2}}$ , which leads to the lower energy pathway (compare Figure S2 in the SI for the alternative pathway). The rotation of the alkene in the perpendicular orientation relative to the square plane of Pd(II) into the plane leads to the alkene insertion transition state for the formation of the new carbon–carbon bond. This step requires an activation free energy of 10.7 kcal/mol and establishes the site- and enantioselectivity of the reaction, and will be discussed in detail below. The product of this step, complex **1**, undergoes a series of rapid isomerizations to form the less stable complex **2**. The transformation of **1** to **2** requires another *cis*–*trans* isomerization because the subsequent reaction pathway with the alkyl chain in the *trans* position to the pyridyl group requires higher free energies of activation (Figure S2 in SI). The *cis*–*trans* isomerization again proceeds through a solvent-assisted pathway in analogy to the one discussed above and is likely to involve several steps. To confirm that these steps are fast for the reasons discussed above, we have calculated intermediate **16** along this isomerization pathway and have found that it is low in energy,

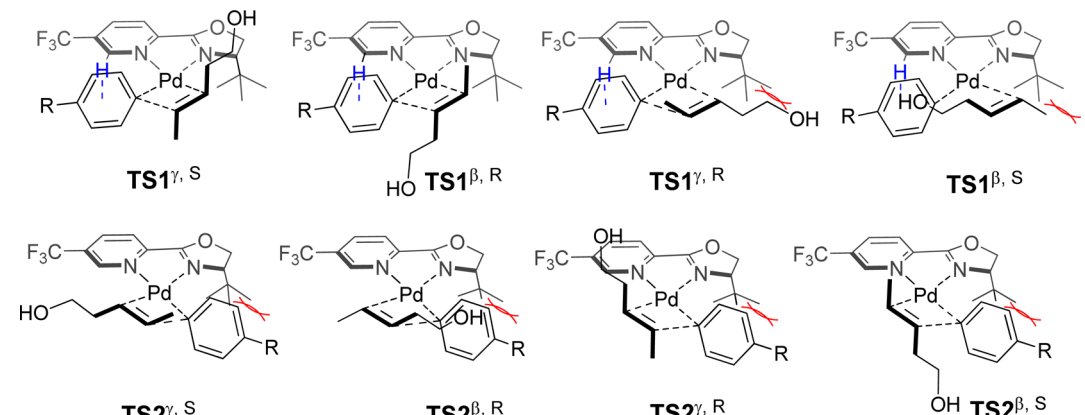
(Scheme S1 in SI), indicating that this isomerization is indeed facile.

It is noteworthy that **1** could in principle form the typical Heck product **13** via TS7 (red pathway in Figure 1). However, this step is predicted to have a free energy of activation of 6.9 kcal/mol for the formation of **11**. Ultimately, the formation of the Heck product is 13 kcal/mol higher in energy than **1**. The formation of the less stable intermediate **11** is reversible. Therefore, the formation of the typical Heck product should occur only to a very small extent, and even this will revert to **1**, reentering the main catalytic sequence.

Intermediate **2** undergoes the first  $\beta$ -hydride elimination via TS3 to form complex **3**. This step requires an activation free energy of 6 kcal/mol. After formation of **3**, the displacement of the alkene from the cationic palladium is calculated to be endothermic by 14.9 kcal/mol and is therefore unlikely to occur. This is presumably due to the electrophilic nature of the palladium cation, which is further enhanced by the electron withdrawing  $\text{CF}_3$  group on the ligand, diminishing the Lewis basic properties of the pyridine. The precise electronic structure of the ligand is therefore crucial for the control of the relay versus the dissociation step and, ultimately, the products formed. These computational results demonstrate the importance of careful ligand design to control the outcome of the reaction. We note that in a more classical Heck reaction, this intermediate would be likely to undergo deprotonation, terminating the cycle and yielding Pd(0). The lack of strong base in the current reaction allows reinsertion and further chain walking.

Intermediate **3** proceeds through a series of repetitive alkene insertion and  $\beta$ -hydride elimination steps. Intermediate **3**

Table 1. Structures and Activation Free Energies of Alkene Insertion Step



The figure shows eight chemical structures of transition states for alkene insertion. They are arranged in two rows of four. The top row shows TS1 isomers: TS1<sup>γ, S</sup>, TS1<sup>β, R</sup>, TS1<sup>γ, R</sup>, and TS1<sup>β, S</sup>. The bottom row shows TS2 isomers: TS2<sup>γ, S</sup>, TS2<sup>β, R</sup>, TS2<sup>γ, R</sup>, and TS2<sup>β, S</sup>. Each structure features a palladium center coordinated by a bidentate ligand with a pyridine ring and an oxazoline ring, and an alkene. A hydroxyl group is also present. Blue dashed lines indicate C-H...O interactions in the TS1 structures.

TS	TS1 <sup>γ,S</sup>	TS1 <sup>β,R</sup>	TS1 <sup>γ,R</sup>	TS1 <sup>β,S</sup>
$\Delta G^\ddagger$ (kcal/mol)	10.7	11.7	13.2	15.0
TS	TS2 <sup>γ,S</sup>	TS2 <sup>β,R</sup>	TS2 <sup>γ,R</sup>	TS2 <sup>β,S</sup>
$\Delta G^\ddagger$ (kcal/mol)	11.8	12.8	13.0	13.4

undergoes alkene reinsertion (TS4) to form complex 4 with an activation free energy of 4.3 kcal/mol. Complex 4 isomerizes to a less stable complex 5, followed by a second  $\beta$ -hydride elimination (TS5) to form the enol palladium hydride complex 6. This step requires an activation free energy of 5.0 kcal/mol. It is noteworthy that this sequence of alkene insertion and  $\beta$ -hydride eliminations, positioning the Pd-carbon bond closer to the oxygen, is energetically downhill as indicated by the comparison of the related species of 2 and 4 or 3 and 6. As will be discussed in more detail later, this is due to the favorable interaction of the negative partial charge on the palladium-bound carbon with the positive partial charge of the carbon bound to the oxygen, providing a thermodynamic driving force for the experimentally observed migration of the double bond.

The final step in this sequence is the formation of the hydroxyalkyl-palladium species 7 where palladium is in the  $\alpha$ -position to the electronegative oxygen. This structure has a relative free energy of  $-9.9$  kcal/mol, which provides a thermodynamic sink to the chain-walking sequence effectively terminating the reaction. The presence of the palladium in the  $\alpha$ -position also increases the acidity of the hydroxyl proton, leading to the final step of oxidative deprotonation by DMF with formation of the final carbonyl product bound to Pd(0). It should be noted that this is likely to be a multistep process and that the reported energies should be considered as upper limits because implicit solvent models will underestimate the solvation stabilization of the protonated DMF. The corresponding deprotonation with DMF could also occur from any other species in the catalytic cycle (Pd-H or  $\beta$ -C-H), but it is equally unfavorable in all cases, and will therefore only occur to a significant extent from 7, which is both the most abundant intermediate and has the kinetically most labile proton. This species can either dissociate to regenerate the catalyst or react directly with another equivalent of the aryl source to close the catalytic cycle. The direct reaction with another substrate will be highly exergonic for the case of release of the very stable molecular nitrogen and still significantly exergonic for the case of the aryl boronic acid substrate. It is therefore the more likely process.

**Selectivity-determining Transition States.** The results depicted in Figure 1 demonstrate that the alkene insertion step

is selectivity-determining. There are eight possible isomeric alkene insertion transition states, which adopt a square-planar geometry. In TS1 and TS2, the aryl group is positioned *trans* and *cis* to chiral oxazoline on the ligand, respectively, which can lead to either of the two constitutional isomers and enantiomers ( $\beta/\gamma$  and (*R*)/(*S*), respectively). We have studied the relative free energies of these eight transition states to elucidate the origin of the experimentally observed site selectively and enantioselectivity.

Our calculations show that the two low energy structures TS1<sup>γ,S</sup> and TS1<sup>β,R</sup> are about 1 kcal/mol more stable than the corresponding TS2s. This is due to the aryl group being positioned perpendicular to the pyridine group on the ligand. This allows a C-H- $\pi$  interaction between the hydrogen and the aryl center (shown in blue dashed lines in Table 1 and Figure 2) with a distance of  $\sim 2.0$  Å. In TS2<sup>γ,S</sup> and TS2<sup>β,R</sup>, the 'Bu

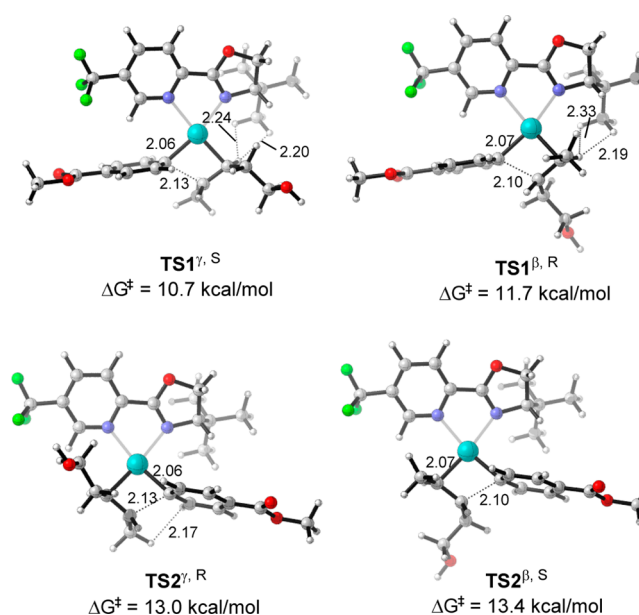


Figure 2. Optimized geometries of the isomers of TS1 and TS2. Bond distances (in Å) and activation free energies are shown.

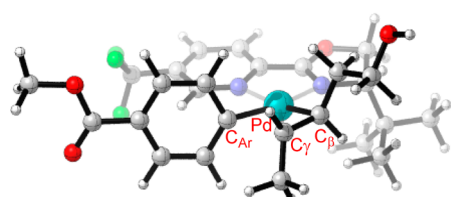


group on the ligand is pointing toward the aryl (shown in red in Table 1), causing steric repulsion and destabilizing **TS2**.<sup>55</sup> Because the isomerization between **IN**<sup>trans-1</sup> and **IN**<sup>cis-1</sup> is fast as discussed earlier, the lowest energy pathway proceeds through **TS1** <sup>$\gamma$ S</sup> with a free energy of activation of 10.7 kcal/mol to form the experimentally observed major product.<sup>24,25</sup>

Conversely, the free energies of the two higher energy transition states leading to the other two constitutional- and stereoisomers are lower for **TS2** <sup>$\gamma$ R</sup> and **TS2** <sup>$\beta$ S</sup> than the corresponding **TS1**s because, in **TS2**, the phenyl group is oriented toward the <sup>t</sup>butyl group with its short axis, making it sterically more favorable than the sp<sup>3</sup> carbon oriented toward the <sup>t</sup>butyl group.

We will start the discussion of these results with an analysis of the factors controlling the site selectivity of the reaction. The second most stable TS, **TS1** <sup>$\beta$ R</sup>, leads to the experimentally observed minor product with different site selectivity and is 1 kcal/mol higher in energy than **TS1** <sup>$\gamma$ S</sup>. The calculated ratio of regioisomers is 5.4:1, which is in good agreement with the experimental value (2.5:1). Although **TS2**s are less favorable than **TS1**s, it is worth noting that the same preference for the C $\gamma$  site selectivity is obtained for **TS2** <sup>$\gamma$ S</sup> (11.8 kcal/mol) and **TS2** <sup>$\beta$ R</sup> (12.8 kcal/mol) for similar reasons. In contrast, the **TS2**s are favored for the higher energy pathways that lead to minor isomers. We will therefore focus most of the following discussion on **TS1**, with brief mention of **TS2**, leading to minor isomers where appropriate. Figure 2 presents the geometries of the four lowest energy transition structures, and Table 2 summarizes key structural and electronic parameters for each.

**Table 2.** NBO Charges and Key Dihedral Angles in **TS1** and **TS2**



	<b>TS1</b> <sup><math>\gamma</math>S</sup>	<b>TS1</b> <sup><math>\beta</math>R</sup>	<b>TS2</b> <sup><math>\gamma</math>R</sup>	<b>TS2</b> <sup><math>\beta</math>S</sup>
charge CH <sub><math>\beta</math></sub>	0.00	0.11	−0.02	0.12
charge CH <sub><math>\gamma</math></sub>	0.12	0.01	0.13	−0.01
C <sub>Ar</sub> –Pd–C <sub><math>\beta</math></sub> –C <sub><math>\gamma</math></sub>	11.1°	15.5°	−16.3°	−17.8°

These results show that the site selectivity is determined by the difference in electronic structure between the two sp<sup>2</sup> carbons. The site selectivity can be understood in terms of an electrophilic interaction of the palladium, leading to a polarization of the alkene in the transition state. The electrons of the alkene form the new Pd–C bond, resulting in almost no net charge change on the Pd-bound alkene carbon, but a buildup of positive charge on the alkene terminus that will become bound to the transferring aryl moiety. An NBO charge analysis indicates that, in the isomers of **TS1**, the alkene carbon forming a bond to Pd is substantially more negative than the carbon forming the bond to the aryl moiety. This negative charge can interact favorably with the positive charge of the oxygen-bound carbon (i.e., with the C–O bond dipole) in the  $\gamma$ -isomers of the TS, but not in the  $\beta$ -isomers. This is in good agreement with an earlier Hammett study of the cationic Heck reaction with styrene substrates, where substituents mostly affected the rate of substitution at the  $\alpha$ -position rather than the

$\beta$ -position.<sup>56</sup> The resulting charge on one alkene terminus interacts with the C–O dipole of the pendant alcohol moiety. The effect will thus disfavor substitution (i.e., formation of a less negative charge) at the alkene terminus closest to the alcohol. We note that this electrostatic interaction will diminish with distance but will give the same expected major constitutional isomer also for homologues of the substrate. This is consistent with the experimentally observed decrease in site selectivity as a function of the chain length and also the correlation presented by one of us using differential <sup>13</sup>C NMR shifts of the alkene carbons.<sup>24,25</sup> Similar trends are obtained for the higher energy **TS2**s, suggesting that the analysis is general.

The results in Table 2 also show a correlation of the geometry with the experimentally observed site selectivity. The ideal dihedral angle C<sub>Ar</sub>–Pd–C <sub>$\beta$</sub> –C <sub>$\gamma$</sub>  (Table 2) is near zero for the square-planar geometry required in the migratory insertion transition state. However, the results show that they are distorted from the ideal geometry as a result of steric repulsion. Table 2 shows that the dihedral angle C<sub>Ar</sub>–Pd–C <sub>$\beta$</sub> –C <sub>$\gamma$</sub>  in **TS1** <sup>$\gamma$ S</sup> is 11.1°, while it increases to 15.5° in **TS1** <sup>$\beta$ R</sup>. In the less favored transition structures, **TS1** <sup>$\gamma$ R</sup> and **TS1** <sup>$\beta$ S</sup>, it is even more distorted from the square-planar geometry. This indicates that steric repulsion also plays a role on site selectivity.

The previously reported results<sup>25</sup> for a series of substituted alkenyl alcohols also demonstrated that steric effects influence the site selectivity, with bulkier groups leading to greater amounts of the  $\gamma$ -insertion product. This is because in the  $\beta$ -insertion transition structure (e.g., **TS1** <sup>$\beta$ S</sup>), increasing the size of the substituent from methyl, which is pointing toward the oxazoline group in **TS1** <sup>$\beta$ S</sup> (Table 2), increases steric repulsion, making this pathway less favorable. This interaction does not occur in **TS1** <sup>$\gamma$ S</sup>, leading to increased site selectivity.

The steric effects for transition structure isomers **TS1** are even more significant for the enantioselectivity of the reaction. The origin of this steric effect becomes clear upon analysis of the geometries shown in Figure 2. In the lowest energy transition structure leading to the minor (*R*)-enantiomer, **TS2** <sup>$\gamma$ R</sup>, the bulkier aryl substituent is pointing toward the <sup>t</sup>Bu group. This suggests that there is significant steric repulsion compared to that for the transition structure leading to the major (*S*)-enantiomer **TS1** <sup>$\gamma$ S</sup> where the hydroxyl ethyl group is pointing away from the <sup>t</sup>Bu group. The dihedral angle C<sub>Ar</sub>–Pd–C–C is −16.3°, significantly larger than that in **TS1** <sup>$\gamma$ S</sup> (11.1°), indicating a steric repulsion in this transition structure. Therefore, the activation free energy is 2.3 kcal/mol higher than that of **TS1** <sup>$\gamma$ S</sup>. This corresponds to an *er* in quantitative good agreement with the experimental observation of 97:3. It should be noted that an analysis of the essentially isoenergetic transition structure **TS1** <sup>$\gamma$ R</sup> where the hydroxymethyl group occupies the position of the aryl group leads to the same result.

This steric effect also explains the enantioselectivity in the other pair of enantioselectivity-determining transition states, **TS1** <sup>$\beta$ R</sup> and **TS2** <sup>$\beta$ S</sup>, due to the steric repulsion between the methyl and <sup>t</sup>butyl group discussed earlier. Although the enantioselectivity of the minor regioisomer has not been determined for this substrate, related minor isomeric products have been reported to have high enantioselectivity,<sup>25</sup> consistent with our prediction.

**Reactivity and Selectivity of *E*- and *Z*-alkenes.** To analyze the dependence of the reaction on substrate geometry, we studied the relative reactivity and selectivity of the (*E*)- and (*Z*)-isomers of hept-4-en-2-ol. It should be noted that the

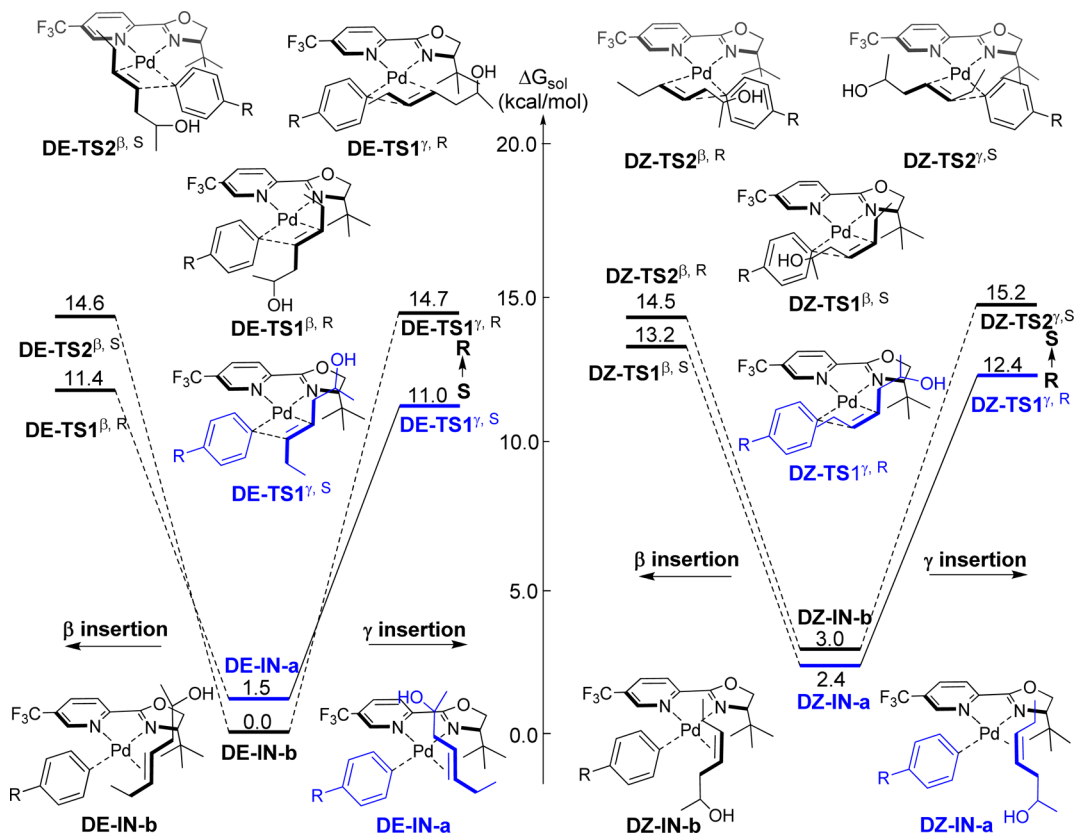


Figure 3. Selectivity-determining transition states for the ethyl-substituted homoallylic secondary alcohols.<sup>57</sup>

coordination of the alkene substrate in IN, the intermediate before the aryl addition transition states, is in rapid equilibrium (Scheme S2 in SI). When (*E*)- and (*Z*)-hept-4-en-2-ol are in a mixture, DE-IN-a, DE-IN-b, DZ-IN-a, and DZ-IN-b in Figure 3 are in equilibrium. This allows the application of the Curtin–Hammett principle, and the reactivity and selectivity of the reaction will be determined by the relative stabilities of the relevant transition structures.

It can be seen from the results in Figure 3 that DZ-IN-a derived from the (*Z*)-isomer, is 2.4 kcal/mol less stable than the lowest energy complex DE-IN-b. This is due to the steric repulsion of the (*Z*)-alkene with the <sup>t</sup>Bu group in DZ-IN-a that cannot be alleviated without inducing a repulsive interaction with the aryl group. As a result, the (*E*)-isomer is predicted to dominate in the equilibrium and react faster than the (*Z*)-isomer through the lowest energy transition state DE-TS1 $^{\gamma, S}$ . However, the site selectivity of the (*Z*)-isomer is with an energy difference of 0.8 kcal/mol predicted to be higher than the site selectivity of the (*E*)-isomer. The enantioselectivity of the (*Z*)-substrate is predicted to be lower than that of the (*E*)-isomer, although both isomers are predicted to give very high enantioselectivity.

The data shown in Figure 3 lead to a series of experimentally verifiable predictions. It is experimentally known that the (*E*)- and the (*Z*)-isomers of hept-4-en-2-ol react in 58% and 79% yield with enantiomeric ratios of 90:10 and 96:4, respectively.<sup>24</sup> Thus, the computational results overestimate the experimentally observed enantioselectivities even though the qualitative prediction of high enantioselectivity is correct.

Although the products of the reaction shown in Figure 3 have been reported previously,<sup>24</sup> the site selectivity for the two substrates has not been disclosed. We have determined the site

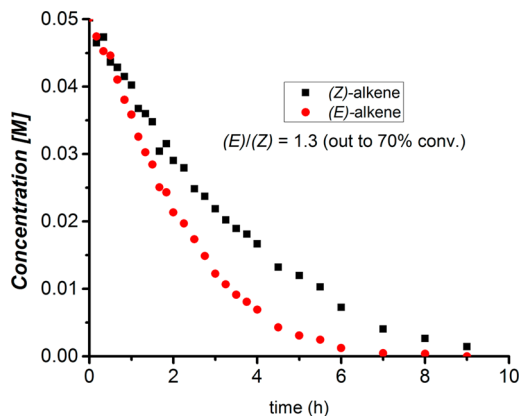


Figure 4. Competition experiment between (*Z*)- and (*E*)-hept-4-en-2-ol.

selectivity for the product derived from the (*Z*)-isomer to be  $\sim 20:1$ , while the one derived from the (*E*)-isomer is 5:1. This is in good agreement with the computational prediction that the (*Z*)-isomer should give high site selectivity.

Finally, we determined the relative reactivity of the two isomers of hept-4-en-2-ol under standard reaction conditions (for experimental details, see SI) in the competition experiment shown in Figure 4. Consistent with the computational predictions, but somewhat counterintuitive based on the inherently higher energy of (*Z*)-alkenes, the (*E*)-alkene is found to react faster than the corresponding (*Z*)-alkene.

## ■ CONCLUSIONS

The mechanism, reactivity, and selectivity of the redox relay, palladium-catalyzed Heck arylation of alkenyl alcohols has been studied by computational and experimental methods. The results for the site selectivity and enantioselectivity for the model substrate (*E*)-pent-3-en-1-ol are in quantitative agreement with the available experimental data and show that migratory insertion is the selectivity-determining step of the reaction. The site selectivity is determined by subtle differences in the electronic structure of the reacting olefin as well as by steric effects that distort the transition structure away from the ideal square planar geometry. The enantioselectivity of the reaction is determined by steric repulsion of the *t*Bu group on the ligand and the aliphatic side chain of the substrate. The final product of the reaction is determined by the electron-withdrawing features of the ligand that make the formation of the traditional Heck product energetically unfavorable. Instead, the favored pathway involves repeated  $\beta$ -hydride eliminations and reinsertions that rapidly equilibrate a series of intermediates with the palladium migrating closer to the electro-negative oxygen. This stabilization of the negative partial charge of the carbon bound to palladium provides a thermodynamic driving force resulting in **7** as the thermodynamic sink. The computational findings are then used to make predictions for a related set of substrates, (*Z*)- and (*E*)-hept-4-en-2-ol. The experimental validation is found to be in good agreement with the computational predictions, including the counterintuitive prediction that the (*Z*)-isomer is more reactive than the (*E*)-isomer.

These results provide detailed mechanistic insights into this novel reaction that expands the synthetic capabilities of this important reaction class to acyclic and electronically minimally biased olefins. The dissection of the different influences on chemo-, site-, and enantioselectivity of the reaction will allow further improvements for cases where the selectivity of the reaction needs to be enhanced. Finally, the atomistic, mechanism-based studies of the stereoselectivity presented here form the basis for Q2MM-based predictions of stereoselectivity<sup>58</sup> that complements the predictive modeling based on widely used physical organic parameters developed by one of us.<sup>42,43</sup>

## ■ ASSOCIATED CONTENT

### Supporting Information

Experimental details, optimized Cartesian coordinates and complete reference 47 for Gaussian 09. This material is available free of charge via the Internet at <http://pubs.acs.org>.

## ■ AUTHOR INFORMATION

### Corresponding Authors

pon@chem.gu.se  
chydwu@ust.hk  
sigman@chem.utah.edu  
owiest@nd.edu

### Notes

The authors declare no competing financial interest.

## ■ ACKNOWLEDGMENTS

We gratefully acknowledge support of this work by the National Science Foundation of China (21133002, 2123201, and 21302006), the MOST of China (2013CB911501), the Shenzhen Peacock Program (KQTD201103), the U.S. National

Science Foundation (NSF CHE 1058075), the Swedish Research Council (Grant No. 2010-4856), and by the FP7-funded SYNFLOW program, ([www.synflow.eu](http://www.synflow.eu)). M.S.S. acknowledges support from the National Institutes of Health (NIGMS RO1 GM063540). We also acknowledge the allocation of computational resources the TeraGrid (TG-CHE090124 and TG-CHE120050) and the Notre Dame Center for Research Computing.

## ■ REFERENCES

- (1) Heck, R. F. *Acc. Chem. Res.* **1979**, *12*, 146.
- (2) De Meijere, A.; Meyer, F. E. *Angew. Chem., Int. Ed. Engl.* **1995**, *33*, 2379.
- (3) Dounay, A. B.; Overman, L. E. *Chem. Rev.* **2003**, *103*, 2945.
- (4) Shibasaki, M.; Vogl, E. M.; Ohshima, T. *Adv. Synth. Catal.* **2004**, *346*, 1533.
- (5) Mc Cartney, D.; Guiry, P. J. *Chem. Soc. Rev.* **2011**, *40*, 5122.
- (6) Berthiol, F.; Doucet, H.; Santelli, M. *Synthesis* **2006**, 1518.
- (7) Pan, D.; Chen, A.; Su, Y.; Zhou, W.; Li, S.; Jia, W.; Xiao, J.; Liu, Q.; Zhang, L.; Jiao, N. *Angew. Chem., Int. Ed.* **2008**, *47*, 4729.
- (8) Cabri, W.; Candiani, I. *Acc. Chem. Res.* **1995**, *28*, 2.
- (9) Andersson, C. M.; Larsson, J.; Hallberg, A. *J. Org. Chem.* **1990**, *55*, 5757.
- (10) Buezo, N. D.; de La Rosa, J. C.; Priego, J.; Alonso, I.; Carretero, J. C. *Chem.—Eur. J.* **2001**, *7*, 3890.
- (11) Itami, K.; Yoshida, J. I. In *The Mizoroki–Heck Reaction*; Oestreich, M., Ed.; Wiley: New York, 2009; p 259.
- (12) Oestreich, M. *Eur. J. Org. Chem.* **2005**, 783.
- (13) Nilsson, P.; Larhed, M.; Hallberg, A. *J. Am. Chem. Soc.* **2003**, *125*, 3430.
- (14) Hu, P.; Kan, J.; Su, W.; Hong, M. *Org. Lett.* **2009**, *11*, 2341.
- (15) Delcamp, J. H.; White, M. C. *J. Am. Chem. Soc.* **2006**, *128*, 15076.
- (16) Su, Y.; Jiao, N. *Org. Lett.* **2009**, *11*, 2980.
- (17) Delcamp, J. H.; Brucks, A. P.; White, M. C. *J. Am. Chem. Soc.* **2008**, *130*, 11270.
- (18) Werner, E. W.; Sigman, M. S. *J. Am. Chem. Soc.* **2010**, *132*, 13981.
- (19) Henriksen, S. T.; Tanner, D.; Skrydstrup, T.; Norrby, P.-O. *Chem.—Eur. J.* **2010**, *16*, 9494.
- (20) Hansen, A. L.; Ebran, J.-P.; Skrydstrup, T.; Ahlquist, M.; Norrby, P.-O. *Angew. Chem., Int. Ed.* **2006**, *45*, 3349.
- (21) Werner, E. W.; Sigman, M. S. *J. Am. Chem. Soc.* **2011**, *133*, 9692.
- (22) Surawatanawong, P.; Hall, M. B. *Organometallics* **2008**, *27*, 6222.
- (23) Datta, G. K.; von Schenck, H.; Hallberg, A.; Larhed, M. *J. Org. Chem.* **2006**, *71*, 3896.
- (24) Werner, E. W.; Mei, T.-S.; Burckle, A. J.; Sigman, M. S. *Science* **2012**, *338*, 1455.
- (25) Mei, T.-S.; Werner, E. W.; Burckle, A. J.; Sigman, M. S. *J. Am. Chem. Soc.* **2013**, *135*, 6830.
- (26) Masllorens, J.; Bouquillon, S.; Roglans, A.; Hénin, F.; Muzart, J. *J. Organomet. Chem.* **2005**, *690*, 3822.
- (27) Barbero, M.; Cadamuro, S.; Dughera, S. *Synthesis* **2006**, 3443.
- (28) Battistuzzi, G.; Cacchi, S.; Fabrizi, G. *Org. Lett.* **2003**, *5*, 777.
- (29) Battistuzzi, G.; Cacchi, S.; Fabrizi, G.; Bernini, R. *Synlett* **2003**, 1133.
- (30) Ambrogio, I.; Fabrizi, G.; Cacchi, S.; Henriksen, S. T.; Frisrup, P.; Tanner, D.; Norrby, P. O. *Organometallics* **2008**, *27*, 3187.
- (31) Henriksen, S. T.; Tanner, D.; Cacchi, S.; Norrby, P. O. *Organometallics* **2009**, *28*, 6201.
- (32) Henriksen, S. T.; Norrby, P. O.; Kaukoranta, P.; Andersson, P. G. *J. Am. Chem. Soc.* **2008**, *130*, 10414.
- (33) Balcells, D.; Maseras, F.; Keay, B. A.; Ziegler, T. *Organometallics* **2004**, *23*, 2784.
- (34) Strömberg, S.; Zetterberg, K.; Siegbahn, P. E. M. *J. Chem. Soc., Dalton Trans.* **1997**, 4147.
- (35) Siegbahn, P. E. M.; Strömberg, S.; Zetterberg, K. *Organometallics* **1996**, *15*, 5542.

- (36) Hii, K. K.; Claridge, T. D. W.; Brown, J. M.; Smith, A.; Deeth, R. *J. Helv. Chim. Acta* **2001**, *84*, 3043.
- (37) Smith, A.; Deeth, R. J.; Hii, K. K.; Brown, J. M. *Tetrahedron Lett.* **1998**, *39*, 3229.
- (38) Deeth, R. J.; Smith, A.; Brown, J. M. *J. Am. Chem. Soc.* **2004**, *126*, 7144.
- (39) Lee, M.-T.; Lee, H. M.; Hu, C.-H. *Organometallics* **2007**, *26*, 1317.
- (40) von Schenck, H.; Åkermark, B.; Svensson, M. *J. Am. Chem. Soc.* **2003**, *125*, 3503.
- (41) Dedieu, A. *Chem. Rev.* **2000**, *100*, 543.
- (42) Sköld, C.; Kleimark, J.; Trejos, A.; Odell, L. R.; Nilsson Lill, S. O.; Norrby, P.-O.; Larhed, M. *Chem.—Eur. J.* **2012**, *18*, 4714.
- (43) Nilsson Lill, S. O.; Ryberg, P.; Rein, T.; Bennström, E.; Norrby, P.-O. *Chem.—Eur. J.* **2012**, *18*, 1640.
- (44) Gøgsig, T. M.; Kleimark, J.; Lill, S. O. N.; Korsager, S.; Lindhardt, A. T.; Norrby, P.-O.; Skrydstrup, T. *J. Am. Chem. Soc.* **2012**, *134*, 443.
- (45) Wu, W.-Q.; Peng, Q.; Dong, D.-X.; Hou, X.-L.; Wu, Y.-D. *J. Am. Chem. Soc.* **2008**, *130*, 9717.
- (46) Zhao, Y.; Truhlar, D. G. *Theor. Chem. Acc.* **2008**, *120*, 215.
- (47) Frisch, M. J. et al. *Gaussian09*; Gaussian: Wallingford, CT, 2009.
- (48) Holder, J. C.; Zou, L.; Marziale, A. N.; Liu, P.; Lan, Y.; Gatti, M.; Kikushima, K.; Houk, K. N.; Stoltz, B. M. *J. Am. Chem. Soc.* **2013**, *135*, 14996.
- (49) Sjögren, M.; Hansson, S.; Norrby, P.-O.; Åkermark, B.; Cucciolito, M. E.; Vitagliano, A. *Organometallics* **1992**, *11*, 3954.
- (50) Johansson, C.; Lloyd-Jones, G. C.; Norrby, P.-O. *Tetrahedron: Asymmetry* **2010**, *21*, 1585.
- (51) Conley, M. P.; Jordan, R. F. *Angew. Chem., Int. Ed.* **2011**, *50*, 3744.
- (52) Haras, A. A.; G. D. W.; Michalak, A.; Rieger, B.; Ziegler, T. *Organometallics* **2006**, *25*, 4491.
- (53) Sabino, A. A.; Machado, A. H. L.; Correia, C. R. D.; Eberlin, M. N. *Angew. Chem., Int. Ed.* **2004**, *43*, 2514.
- (54) Machado, A. H. L.; Milagre, H. M. S.; Eberlin, L. S.; Sabino, A. A.; Correia, C. R. D.; Eberlin, M. N. *Org. Biomol. Chem.* **2013**, *11*, 3277.
- (55) Conversely, the two high-energy isomers of **TS1** are slightly higher in energy than their **TS2** counterparts because of the stronger repulsion of the <sup>t</sup>Bu group with the methyl group compared to that of the aryl ring.
- (56) Fristrup, P.; Le Quement, S.; Tanner, D.; Norrby, P.-O. *Organometallics* **2006**, *23*, 6160.
- (57) Note that the (*E*)- and (*Z*)-isomers lead to opposite enantiomers as indicated in the nomenclature of the relevant transition structures.
- (58) Donoghue, P. J.; Helquist, P.; Norrby, P.-O.; Wiest, O. *J. Am. Chem. Soc.* **2009**, *131*, 410.

## ■ NOTE ADDED IN PROOF

An alternative study of the same reaction was recently published: Dang, Y.; Qu, S.; Wang, Z.-X.; Wang, X. *J. Am. Chem. Soc.* **2014**, *136* (3), 986–998.

## ■ NOTE ADDED AFTER ASAP PUBLICATION

Scheme 2 was incorrect in the version published ASAP January 22, 2014; the correct version reposted January 23, 2104. NOTE ADDED IN PROOF was added January 24, 2014.